Jun-Yeop Lee[a], Marika Vespa, Xavier Gaona, Kathy Dardenne, Jörg Rothe, Thomas Rabung, Marcus Altmaier and Jong-Il Yun*

Formation, stability and structural characterization of ternary $MgUO_2(CO_3)_3^{2-}$ and $Mg_2UO_2(CO_3)_3(aq)$ complexes

DOI 10.1515/ract-2016-2643
Received June 9, 2016; accepted October 4, 2016; published online November 9, 2016

Abstract: The formation of ternary Mg-UO_2-CO_3 complexes under weakly alkaline pH conditions was investigated by time-resolved laser fluorescence spectroscopy (TRLFS) and extended X-ray absorption fine structure (EXAFS) and compared to Ca-UO_2-CO_3 complexes. The presence of two different Mg-UO_2-CO_3 complexes was identified by means of two distinct fluorescence lifetimes of 17 ± 2 ns and 51 ± 2 ns derived from the multi-exponential decay of the fluorescence signal. Slope analysis in terms of fluorescence intensity coupled with fluorescence intensity factor as a function of log [Mg(II)] was conducted for the identification of the Mg-UO_2-CO_3 complexes forming. For the first time, the formation of both $MgUO_2(CO_3)_3^{2-}$ and $Mg_2UO_2(CO_3)_3(aq)$ species was confirmed and the corresponding equilibrium constants were determined as $\log \beta^0_{113} = 25.8 \pm 0.3$ and $\log \beta^0_{213} = 27.1 \pm 0.6$, respectively. Complementarily, fundamental structural information for both Ca-UO_2-CO_3 and Mg-UO_2-CO_3 complexes was gained by extended EXAFS revealing very similar structures between these two species, except for the clearly shorter U-Mg distance (3.83 Å) compared with U-Ca distance (4.15 Å). These results confirmed the inner-sphere character of the Ca/Mg-UO_2-CO_3 complexes. The formation constants determined for $MgUO_2(CO_3)_3^{2-}$ and $Mg_2UO_2(CO_3)_3(aq)$ species indicate that ternary Mg-UO_2-CO_3 complexes contribute to the relevant uranium species in carbonate saturated solutions under neutral to weakly alkaline pH conditions in the presence of Mg(II) ions, which will induce notable influences on the U(VI) chemical species under seawater conditions.

Keywords: Uranium, carbonate, ternary complex, chemical thermodynamic data, time-resolved laser fluorescence spectroscopy, extended X-ray absorption fine structure.

1 Introduction

Various geochemical reactions, such as ligand complexation, sorption, and formation of colloid/pseudo-colloid species, govern the migration behavior of actinide elements. Therefore, a detailed and comprehensive understanding of the chemical behavior of actinides is of cardinal importance for the accurate prediction of radionuclide migration in deep geologic repositories, and accordingly, for the long-term safety assessment of these underground facilities [1].

Recently, the formation behavior and the reaction characteristics of ternary uranium carbonate species relevant to various earth-alkaline metal ions were intensively investigated. This interest is driven by the remarkably large stability field of these U(VI) species [2], together with relatively abundant amounts of carbonate and Ca(II)/Mg(II) ions in natural groundwater and seawater systems [3, 4].

Since Bernhard et al. [5] reported the existence of the ternary aqueous $Ca_2UO_2(CO_3)_3(aq)$ species, the formation and chemical behavior of Ca-UO_2-CO_3 species have been investigated with various analytical methods such as time-resolved laser fluorescence spectroscopy (TRLFS) [2, 6–8], laser-induced photoacoustic spectroscopy (LPAS) [7], ion exchange method [9], optical absorption spectroscopy [10], and extended X-ray absorption fine structure (EXAFS) [7, 11]. Owing to particular experimental difficulties and uncertainties in the precise chemical speciation of ternary U(VI) carbonate complexes, only a few researches have reported the formation constants of ternary Ca-UO_2-CO_3 species [2, 7–9]. Chemical thermodynamic data revealed the predominant presence of those complexes in natural

[a]Present address: Institute for Nuclear Waste Disposal, Karlsruhe Institute of Technology, Postfach 3640, 76021 Karlsruhe, Germany
***Corresponding author: Jong-Il Yun,** Department of Nuclear and Quantum Engineering, KAIST, 291 Daehak-ro, Yuseong-gu, Daejeon 34141, Republic of Korea, E-mail: jiyun@kaist.ac.kr
Jun-Yeop Lee: Department of Nuclear and Quantum Engineering, KAIST, 291 Daehak-ro, Yuseong-gu, Daejeon 34141, Republic of Korea
Marika Vespa, Xavier Gaona, Kathy Dardenne, Jörg Rothe, Thomas Rabung and Marcus Altmaier: Institute for Nuclear Waste Disposal, Karlsruhe Institute of Technology, Postfach 3640, 76021 Karlsruhe, Germany

groundwater conditions with moderately high carbonate and Ca(II) ion concentrations [8]. The formation of these species can notably affect the U(IV)/U(VI) redox distribution in certain scenarios/concepts relevant in the framework of radioactive waste disposal.

The aqueous speciation of uranium under seawater conditions has gained relevance in the last decade due to environmental issues, but also because of its possible recovery as alternative to terrestrial mining [10, 12]. In this context, not only Ca-UO_2-CO_3 but also other ternary uranium species need to be considered, especially in view of the relatively high Mg(II) concentrations ([Mg(II)] ≈ 0.055 M) omnipresent in seawater [3].

Besides Ca-UO_2-CO_3 species, only a few spectroscopic properties and chemical thermodynamic data are available for ternary Mg(II) uranium carbonate species. Dong and Brooks [9] investigated the formation behavior of Mg-UO_2-CO_3 species by using ion exchange method at weakly basic conditions. The authors identified the presence of the $MgUO_2(CO_3)_3^{2-}$ species and determined the formation constant to be log $\beta^0_{113} = 26.11 \pm 0.04$ at I = 0 M. Spectroscopic properties such as fluorescence peak positions and fluorescence lifetime associated with the $MgUO_2(CO_3)_3^{2-}$ species were reported by Geipel et al. [2] by means of TRLFS. The spectroscopic data of Mg-UO_2-CO_3 species showed almost indistinguishable characteristics compared with those of Ca-UO_2-CO_3 species, except a slightly increased fluorescence lifetime for the $MgUO_2(CO_3)_3^{2-}$ species (18.2 ± 2.7 ns) [2]. At the same time, Geipel et al. [2] reported log $\beta^0_{113} = 26.24 \pm 0.13$, which agrees well with the data from Dong and Brooks [9]. Recently, Endrizzi and Rao [10] have reported the formation behavior and chemical thermodynamic data of the ternary Mg-UO_2-CO_3 species by means of spectrophotometric titrations. The formation constant of $MgUO_2(CO_3)_3^{2-}$ was assessed to be log $\beta^0_{113} = 26.25 \pm 0.04$ at I = 0 M [10]. All of the accessible formation constants regarding the $MgUO_2(CO_3)_3^{2-}$ species showed an excellent agreement with each other. However, to the best of our knowledge, no literature studies have reported the existence of the second Mg-UO_2-CO_3 complex, even though the presence of $Mg_2UO_2(CO_3)_3(aq)$ species is strongly anticipated, and the formation of all $Me_2UO_2(CO_3)_3(aq)$ (Me = Ca, Ba, Sr) species for other earth-alkaline metal ions have been already reported [2, 9]. In addition, Endrizzi and Rao [10] stated that the difficulty in the exact identification of the chemical speciation of the $Mg_2UO_2(CO_3)_3(aq)$ species might be caused by relatively small formation constants of Mg-UO_2-CO_3 complexes. A precise determination of the chemical behavior of $Mg_2UO_2(CO_3)_3(aq)$ may play an important role in the exact determination of the uranium speciation, especially in seawater conditions owing to the high Mg(II) ion concentration in those systems (≈ 0.055 M) [3].

Besides the investigation of their thermodynamic properties, a study on fundamental structural information to substantiate the actual formation of ternary uranium carbonate species has been scarcely conducted. Bernhard et al. [7] and Kelly et al. [11] confirmed the presence of Ca-UO_2-CO_3 complexes by U L_{III}-edge EXAFS data. Meanwhile, the structural information of Mg-UO_2-CO_3 species was theoretically predicted with molecular dynamic simulation by Kerisit and Liu [13], who reported molecular structures for Mg-UO_2-CO_3 complexes very similar to those of Ca-UO_2-CO_3 species except for the distances between U-Mg (3.74 Å for $MgUO_2(CO_3)_3^{2-}$) and U-Ca (4.05 Å for $CaUO_2(CO_3)_3^{2-}$). To the best of our knowledge, no EXAFS study on the Mg-UO_2-CO_3 system was performed so far. Thus, the exact structural information of ternary Mg-UO_2-CO_3 species remains to be unambiguously characterized.

In this framework, the main objective of the present work is to investigate the formation behavior of ternary Mg-UO_2-CO_3 complexes under weakly alkaline pH conditions. Spectroscopic characteristics such as fluorescence peak positions and fluorescence lifetimes of Mg-UO_2-CO_3 species with respect to the exact chemical speciation of ternary uranium complexes were obtained by means of TRLFS. Furthermore, the structural information for both Ca-UO_2-CO_3 and Mg-UO_2-CO_3 species was evaluated by EXAFS at the U L_{III}-edge. The investigation of the Ca-UO_2-CO_3 complexes aimed at allowing a comparison of the magnesium system with a more clearly established system. For the first time, the $Mg_2UO_2(CO_3)_3(aq)$ species was identified based on advanced spectroscopic techniques (TRLFS and EXAFS), and the corresponding stability constant derived through a slope analysis using fluorescence intensities and fluorescence intensity factors. This work complements previously reported data on the Ca-UO_2-CO_3 and Mg-UO_2-CO_3 systems, and allows a more accurate description of the aqueous speciation of U(VI) in seawater conditions.

2 Experimental section

2.1 Sample preparation

All experiments were performed under aerobic conditions at 23 ± 2 °C. All chemicals utilized in the present work were of analytical grade. The stock solution of U(VI) was prepared by dissolution of $UO_2(NO_3)_2 \cdot 6H_2O$ (Merck) in 2 M HNO_3 (Sigma-Aldrich, 99.999+ %). The U(VI) stock solution was purified by means of the sequential precipitation method

to eliminate impurities. The concentration of aqueous U(VI) was set at 10^{-3} M by adding deionized water obtained from a water purification system (Millipore, Milli-Q/RiOs). The pH of the sample was maintained at 8.2 using a buffer solution of 5×10^{-2} M TRIS (Sigma-Aldrich, ≥ 99.9%) and HCl (Sigma-Aldrich, 99.999%). Total concentration of inorganic carbon was initially set to 5×10^{-2} M with Na_2CO_3 (Sigma-Aldrich, 99.999%). Although this concentration was greater than the carbonate concentration in equilibrium with the open atmosphere, no relevant degassing of the resulting solutions was observed. The Mg(II) ion concentration ranged between 1.7 mM and 39.2 mM, and was achieved by dilution of a 1.0 M $MgCl_2{\cdot}6H_2O$ (Sigma-Aldrich, 99.995%) stock solution. Ionic strength was maintained at 0.15 M NaCl–$NaHCO_3$–Na_2CO_3 (Sigma-Aldrich, ≥ 99.999%) except for the samples with the highest Mg(II) ion concentration (17.0 mM ≤ [Mg(II)] ≤ 39.2 mM), where $MgCl_2$ imposes ionic strength up to 0.29 M. These conditions were necessary to assess the formation of the higher Mg-UO_2-CO_3 complex. Aqueous U(VI) and Mg(II) concentrations were determined after ultra-filtration with 10 kD (2–3 nm) membrane filters (Millipore, Amicon Ultra-15) using inductively coupled plasma mass spectrometry (ICP-MS) and inductively coupled plasma optical emission spectrometry (ICP-OES), respectively. Concentrations of U(VI) and Mg(II) after ultra-filtration were used for the interpretation of the data, instead of the corresponding initial concentrations, although only minor variations (< 14%) between both values were observed within the timeframe of the experiments (10 days). No remarkable difference in the concentration of Mg(II) ion was observed before and after ultrafiltration, indicating that there was no significant formation of Mg(II) solid phases in the course of the experiments, in spite of oversaturation conditions with respect to the thermodynamically most stable but often kinetically hindered $MgCO_3$(s) reached in the samples with highest [Mg(II)]. This is consistent with previous observations reported in the literature, indicating the formation of $MgCO_3{\cdot}3H_2O$(s) (*ca.* 2 orders of magnitude more soluble than $MgCO_3$(s), see Table A1) at $T = 25$ °C and $P = 1$ bar [14].

The aqueous U(VI) samples for the EXAFS investigations were prepared as described above, except for earth-alkaline metal ion concentrations and pH. The pH of samples was maintained at pH = 8.0 using 5×10^{-2} M TRIS buffer (Sigma-Aldrich, 99.9%) and HCl (Merck). Total concentrations of earth-alkaline metal ions (Mg(II) and Ca(II)) were controlled in the range of 6 mM–104 mM by dilution of 1.0 M $CaCl_2{\cdot}2H_2O$ (Merck, 99.0–102.0%) or 1.0 M $MgCl_2{\cdot}6H_2O$ (Merck, 99.0–101.0%) stock solution. For the EXAFS measurements, the samples were ultrafiltered with a membrane filter of 10 kD (2–3 nm) (Pall Life Sciences). Aqueous U(VI) and Mg(II)/Ca(II) ion concentrations were measured with ICP-MS/OES, revealing slight decrement in aqueous U(VI) concentration (*ca.* 15%) and very minor presence of a solid phase in the present system. These metastable conditions were forced to retain a sufficiently high U(VI) concentration in solution, needed to perform accurate EXAFS investigations with good counting statistics. In addition, a sample without earth-alkaline metal ions was prepared and used as reference.

2.2 Instruments

Aqueous U(VI) samples were excited by using a pulsed laser beam of a Nd : YAG laser (Quantel Brilliant B, pulse duration: 6 ns, repetition rate: 10 Hz). The fourth harmonic (266 nm) of the Nd : YAG laser was used for the TRLFS measurements. The laser pulse energy was 2.9 ± 0.1 mJ and monitored by laser energy meter (Gentec·eo, XLD 12-1S-H2-DO). The fluorescence emission was collected by the customized bundle-type optical fiber (Fiberguide) and then delivered to the Czerny-Turner spectrometer (Andor, SR-303i-A) coupled with ICCD camera (Andor, DH734-18F-C3). The gate delay and the gate width of the ICCD camera were monitored continuously with an oscilloscope (Tektronix, TDS 380P). The spectral response of the entire detection system including optical fiber, spectrometer, and ICCD camera was calibrated and corrected with a fluorescence standard reference material (NIST, SRM 936a). The fluorescence measurement window for aqueous U(VI) complexes was set to the wavelength range of 450 nm–590 nm. The data evaluation of the fluorescence signal collected in the present work was conducted with commercial software programs: GRAMS/AI (Thermo Scientific) and MATLAB (Mathworks). A detailed description of the TRLFS equipment is given elsewhere [8].

2.3 Bulk-EXAFS data collection and reduction

Bulk-EXAFS data at the U L_{III}-edge were collected at the INE-Beamline at the Ångströmquelle Karlsruhe (ANKA) [15]. The beamline is equipped with a Ge(422) double crystal monochromator (DCM) coupled with a collimating and a focusing Rh coated mirrors before and after the DCM, respectively. The monochromator is calibrated for the U L_{III}-edge by assigning the energy of 17,038 eV to the first inflection point of the K-edge absorption spectrum of the Y metal foil. All measurements were recorded at room

temperature in fluorescence mode using a multi-element Ge-detector.

All EXAFS spectra were extracted from raw data with the Athena interface of the IFFEFIT software [16, 17]. The Fourier transforms (FTs) were obtained from the k^3-weighted $\chi(k)$ functions using a Kaiser-Bessel window function with an apodization parameter of 1. Multishell fits were performed in real space in the range from 1 to *ca.* 4.3 Å. Amplitude and phase shifts functions were calculated using the FEFF 8.4 code [18]. The amplitude reduction factor S_0^2 was set to the value of 1 [19].

2.4 Thermodynamic background

Thermodynamic data used for speciation calculations were mostly taken from the OECD-NEA thermodynamic database [20]. Additionally, equilibrium constants for Ca-UO_2-CO_3 complexes were obtained from previous literature data [8]. Thermodynamic data reported for the binary systems Ca-CO_3 and Mg-CO_3 were considered [21] to assess the total and free concentration of Ca(II) and Mg(II) in the system, respectively. Chemical reactions and corresponding equilibrium constants used in the present work are listed in Table A1 in the Appendix.

The specific ion interaction theory (SIT) [22, 23] (SIT) was used for the extrapolation of thermodynamic data derived at higher ionic strength conditions to I = 0 M. Based on the SIT formulism, the activity coefficient of the ionic species *i* (γ_i) at given ionic strength can be expressed as:

$$\log \gamma_i = -z_i^2 D + \sum \varepsilon(i, j) m_j \quad (1)$$

where z_i is the charge of ion i, $\varepsilon(i, j)$ is the specific ion interaction parameter for a pair of oppositely charged ions, m_j is the molal concentration of ion j, D is the Debye-Hückel term ($D = (0.509\sqrt{I})/(1 + Bå\sqrt{I})$ at 25 °C, with Bå = 1.5), and I is the ionic strength. In the present work, not only NaCl–$NaHCO_3$–Na_2CO_3 but also NaCl–$NaHCO_3$–Na_2CO_3–$MgCl_2$ mixtures were used as background electrolytes. In these systems, activity coefficients of cationic and anionic species can be calculated according to the eqs. (2) and (3), respectively:

$$\log \gamma_M = -z_M^2 D + \varepsilon(M, Cl^-) m_{Cl^-} \quad (2)$$

$$\log \gamma_X = -z_X^2 D + \varepsilon(X, Na^+) m_{Na^+} + \varepsilon(X, Mg^{2+}) m_{Mg^{2+}} \quad (3)$$

SIT ion interaction coefficients for all ionic species relevant in the Mg-UO_2-CO_3 system investigated in this work were previously reported in the literature, except for $\varepsilon(MgUO_2(CO_3)_3^{2-}, Na^+)$ and $\varepsilon(MgUO_2(CO_3)_3^{2-}, Mg^{2+})$. Using the concept of chemical analogy, $\varepsilon(MgUO_2(CO_3)_3^{2-}, Na^+) = -0.02 \pm 0.09$ kg·mol^{-1} was adopted in this work based on the SIT ion interaction coefficients previously reported for $UO_2(CO_3)_2^{2-}$ and $CaUO_2(CO_3)_3^{2-}$ species [8, 20]. The assignment of SIT ion interaction coefficients for M^{2+} - X^{2-} ion combinations is hindered by their tendency to associate. Considering the low coefficient derived for the interaction between $MgUO_2(CO_3)_3^{2-}$ and Na^+, a value of $\varepsilon(MgUO_2(CO_3)_3^{2-}, Mg^{2+}) = 0.0 \pm 0.2$ kg·mol^{-1} is proposed in the present work. Similar $\varepsilon(i, j)$ values for the interaction of X^{2-} species with Na^+ and Ca^{2+} have been reported in the literature [24]. Note further that within the experimental conditions considered in this study (0.10 M ≤ [Na^+] ≤ 0.12 M; [Mg^{2+}] ≤ 0.04 M; 0.15 M ≤ I ≤ 0.29 M), the SIT expression for the calculation of activity coefficients is mainly dominated by the Debye-Hückel term, whereas the impact of the short range, non-electrostatic interactions represented by the term $\sum \varepsilon(i, j) \cdot m_j$ is relatively small.

3 Results and discussion

3.1 Characterization and formation of the Mg-UO_2-CO_3 complexes by TRLFS

As a result of the TRLFS study, Figure 1 shows the U(VI) fluorescence spectra in presence of carbonate and various Mg(II) ion concentrations. The U(VI) sample without Mg(II) ions exhibited individually well-resolved fluorescence peaks. The blue-shifted fluorescence peaks relative to the un-complexed UO_2^{2+} ions [25] were observed at 467, 485, 506, 528, and 551 nm by means of peak deconvolution with Voigt peak fitting [26]. The measured fluorescence peak positions at [Mg(II)] = 0 M are in a good accordance with the spectroscopic properties of the $UO_2(CO_3)_3^{4-}$ species, [8, 27] which is known to be the major U(VI) species at weakly alkaline pH and in carbonate saturated solutions without any earth-alkaline metal ions [20]. In addition, the U(VI) fluorescence intensity increases with increasing Mg(II) concentration, indicating a chemical reaction between Mg(II) ions and U(VI) species, which is a substantial evidence of the formation of Mg(II)-bound U(VI) species. Additional U(VI) species formed in the present work can be assigned to Mg-UO_2-CO_3 complexes by the corresponding fluorescence peak wavelengths, which agree well with data reported by Geipel et al. [2].

Figure 2a represents in detail the increase in fluorescence intensity at gate delay time $\Delta t_d = 0$ ns and at gate width $\Delta t_w = 50$ ns as a function of log [Mg(II)]. In addition,

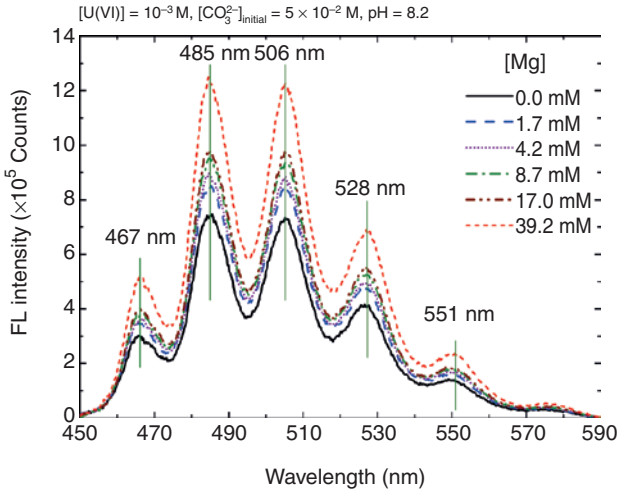

Figure 1: Fluorescence spectra of the UO_2-CO_3 and Mg-UO_2-CO_3 complexes at pH = 8.2 and various Mg(II) ion concentrations. Gate delay $\Delta t_d = 0$ ns; Gate width $\Delta t_w = 50$ ns.

the fluorescence shape and peak wavelengths remained almost constant at various Mg(II) ion concentrations at pH = 8.2, as shown in Figure 2b. The only difference in the measured fluorescence wavelengths of those U(VI) species was the fluorescence peak width, which slightly narrows at higher Mg(II) ion concentration. The relationship between fluorescence peak width and earth-alkaline metal ion concentration for the Mg-UO_2-CO_3 species is in relatively good agreement with those for Ca-UO_2-CO_3 species [8]. The overall spectroscopic properties of Mg-UO_2-CO_3 complexes are similar to the analog Ca-UO_2-CO_3 species, except for the fluorescence lifetimes, which will be discussed later.

Figure 3a shows the time-resolved fluorescence intensities of mixtures of binary UO_2-CO_3 and ternary Mg-UO_2-CO_3 complexes measured at various Mg(II) concentrations. Multi-exponential decay of fluorescence intensity from different U(VI) carbonate species was observed at pH = 8.2 by means of TRLFS.

In general, the fluorescence intensity of a chemical species follows the single exponential decay equation, as expressed in eq. (4),

$$FI = FI_0 \cdot e^{\left(-\frac{t}{\tau}\right)} \tag{4}$$

where t is the gate delay time, FI is the fluorescence intensity at specific gate delay time t, FI_0 is FI at gate delay time t = 0, and τ is the fluorescence lifetime of the chemical species. The expression in eq. (4) is converted into semi-logarithmic scale in eq. (5). Consequently, the fluorescence lifetime τ can be evaluated in terms of the inversed slope of the logarithmic fluorescence intensity function:

$$\ln(FI) = \ln(FI_0) - \frac{t}{\tau} \tag{5}$$

In the presence of mixtures of different species, multi-exponential decay curves are obtained if the ligand exchange reaction rate is slow compared to the fluorescence decay

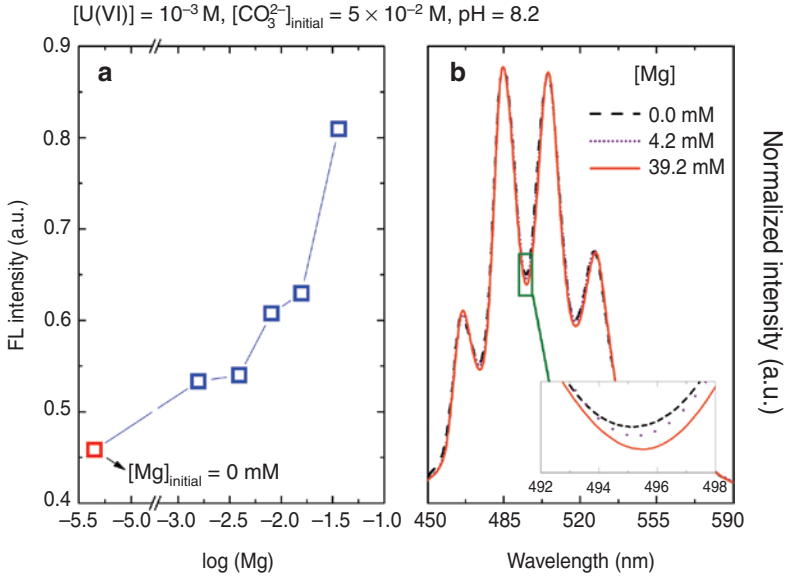

Figure 2: (a) Fluorescence intensities of UO_2-CO_3 and Mg-UO_2-CO_3 complexes as a function of log [Mg(II)] at [U(VI)] = 10^{-3} M. Traceable amount of Mg(II) ion at $[Mg(II)]_{initial} = 0$ mM is owing to the minor impurity. Gate delay $\Delta t_d = 0$ ns; Gate width $\Delta t_w = 50$ ns. (b) Normalized fluorescence spectra of UO_2-CO_3 and Mg-UO_2-CO_3 complexes at pH = 8.2 and with increasing Mg(II) ion concentrations.

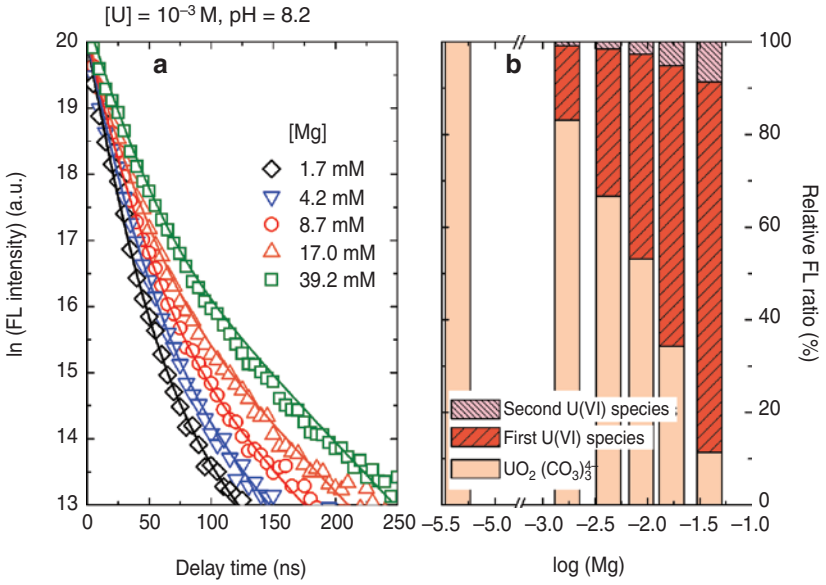

Figure 3: (a) Time-dependent fluorescence intensities of the UO_2-CO_3 and Mg-UO_2-CO_3 complexes measured at pH = 8.2 and various Mg(II) ion concentrations. Gate width $\Delta t_w = 50$ ns. (b) Relative fluorescence intensity ratios between various U(VI) species as a function of Mg(II) ion concentration.

rate of the excited state (otherwise mono-exponential decay curves are obtained). The individual fluorescence lifetimes of pure chemical species can be determined by linearly fitting of the fluorescence decay curves.

Due to substantial differences among the fluorescence lifetimes of the individual U(VI) complexes formed in the present work, a fairly clear multi-exponential tendency was observed by TRLFS. Note that this observation is in contrast with previous studies available for the ternary system Ca-UO_2-CO_3, [8] where only a mono-exponential decay was observed. The fluorescence lifetimes of all U(VI) carbonate species were determined according to eqs. (4) and (5). The characteristic fluorescence lifetime of the $UO_2(CO_3)_3^{4-}$ species was evaluated to be 9 ± 1 ns from the fluorescence signal at low Mg(II) concentrations (0–8.7 mmol/L), in good agreement with previous literature data [8, 27]. For the same Mg(II) ion concentration range, a relatively long fluorescence lifetime of 17 ± 2 ns was also calculated from the linear fit of the multi-exponential curve, corresponding to the first ternary Mg-UO_2-CO_3 complex. The obtained fluorescence lifetime of the Mg-UO_2-CO_3 species was in good accordance with the lifetime of $MgUO_2(CO_3)_3^{2-}$ species (18.2 ± 2.7 ns) reported by Geipel et al. [2]. Based on the increasing fluorescence intensity with Mg(II) concentrations, the fluorescence peak wavelengths, and the fluorescence lifetime resolved from the multi-exponential decay curve, the Mg-UO_2-CO_3 complex formed at low Mg(II) concentrations (0–8.7 mmol/L) was assigned to the $MgUO_2(CO_3)_3^{2-}$ species. Besides the $MgUO_2(CO_3)_3^{2-}$ species, the presence of a further complexed Mg-UO_2-CO_3 species at higher Mg(II) concentrations (8.7 mM ≤ [Mg(II)] ≤ 39.2 mM) was observed with a characteristic fluorescence lifetime of 51 ± 2 ns. The spectroscopic properties of this species were almost identical to those of $UO_2(CO_3)_3^{4-}$ and $MgUO_2(CO_3)_3^{2-}$ species, except for the fluorescence lifetime. This is clearly related to the identical first coordination sphere of uranium in these binary/ternary species.

Relative fluorescence intensity ratios among $UO_2(CO_3)_3^{4-}$ and Mg-bound U(VI) species were evaluated at various Mg(II) ion concentrations according to the best-fit of multi-exponential fluorescence decay curves based on the fluorescence lifetimes of each U(VI) species. As represented in Figure 3b, the U(VI) species having a longer fluorescence lifetime could be attributed to be the $Mg_2UO_2(CO_3)_3(aq)$ species as it correlated to increasing Mg(II) ion concentrations in analogy with previous evidences reported for Ca(II), Ba(II) and Sr(II). However, due to the lack of literature data on the exact chemical behavior and the spectroscopic characteristics of $Mg_2UO_2(CO_3)_3(aq)$ species, the Mg(II)-bound U(VI) species observed at higher Mg(II) concentration cannot be unambiguously assigned to the second Mg-UO_2-CO_3 species as $Mg_2UO_2(CO_3)_3(aq)$. A detailed description with respect to the determination of the precise stoichiometry of Mg(II) in this U(VI) carbonate complex is provided in the section of "Chemical and thermodynamic models".

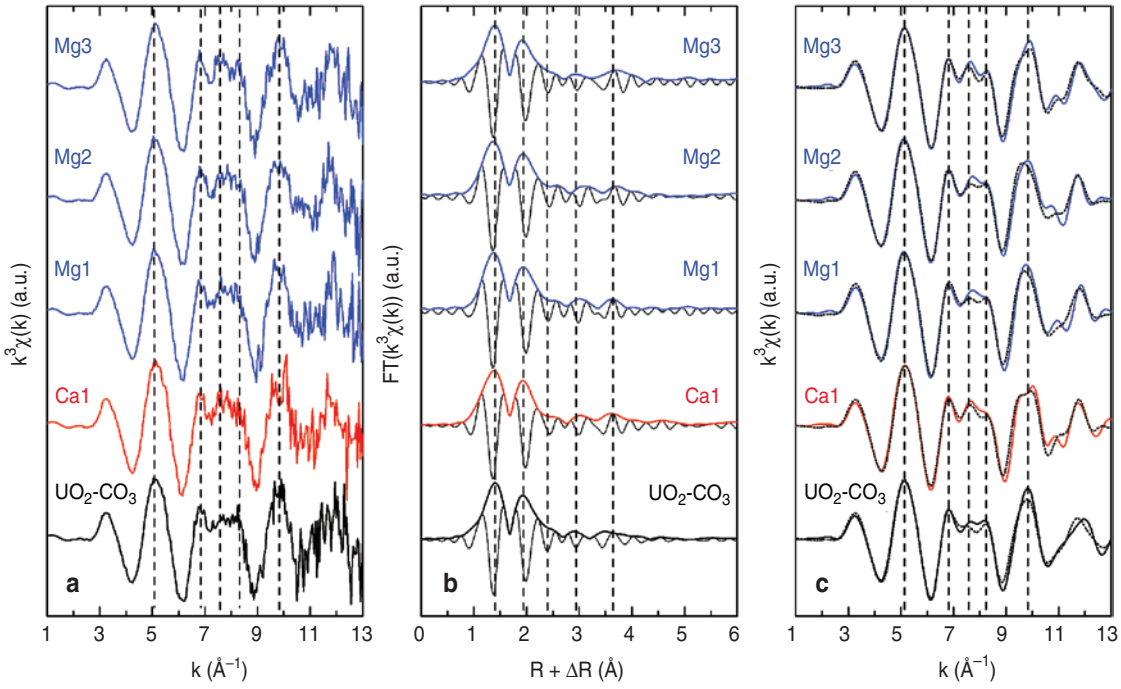

Figure 4: U L_{III}-edge experimental spectra of the reference UO_2-CO_3 sample along with the Ca-UO_2-CO_3 sample (Ca1) and Mg-UO_2-CO_3 samples (Mg1, Mg2, and Mg3) for (a) k^3-weighted, normalized, background-subtracted EXAFS spectra; (b) Radial Structure Functions (modulus and imaginary parts) obtained from the Fourier transform of the EXAFS spectra presented in Figure 4a; (c) experimental (solid line) and theoretical (dashed line) k^3-weighted EXAFS function of the Fourier-backtransform spectra ($R+\Delta R = ca.$ 1.0–4.5 Å). Details of the sample preparation and composition are given in Table 2.

3.2 Characterization of Ca/Mg-UO_2-CO_3 complexes by EXAFS

The normalized, background-subtracted k^3-weighted $\chi(k)$ EXAFS spectra of the U(VI) carbonate complexes free of earth-alkaline metal ion as well as with Ca(II) and varying Mg(II) ion concentrations are shown in Figure 4a. All k^3-weighted $\chi(k)$ spectra are very similar. The major differences are observed in the range from *ca.* 6.5 to 8.5 $Å^{-1}$. This beat pattern shows an elongated upward oscillation ending with a tip at 6.8 $Å^{-1}$, followed by the splitting of the oscillation with maxima at 7.6 and 8.2 $Å^{-1}$, especially observable in the complex with highest Mg(II) ion concentration, which is relatively comparable to the one observed from Kelly and co-workers [19] on the similar system, in which the Ca(II) ion concentration varied.

Radial structure functions [modulus, |FT|, and imaginary parts, ImFT] (RSF, Figure 4b) obtained from the Fourier transform of the k^3-weighted $\chi(k)$ of all EXAFS spectra display strong similarities up to *ca.* $R+\Delta R = 2.5$ Å and distinct differences at larger distances. The first two shells at *ca.* $R+\Delta R = 1.4$ Å and 1.9 Å are comparable in all samples, indicating the presence of axial and equatorial oxygen atoms. At *ca.* $R+\Delta R = 2.4$ Å, a very small shift to longer distances is observed in the RSF-ImFT of the Ca- and Mg-containing samples compared to the pure U(VI)-carbonate complex. The $R+\Delta R$ region between 2.7 and 4.0 Å shows the greatest changes in the presence of Ca(II) or Mg(II) ions. In this same region, the RSF-|FT| indicates two asymmetric peaks with maxima shifting to longer distances in the presence of the earth-alkaline metal ions and increasing Mg(II) ion concentration.

Data analysis was further performed using the Fourier backtransform (FT^{-1}) spectra in the range from *ca.* 1.0 to 4.5 Å. Experimental (solid line) and theoretical (dashed line) spectra are shown in Figure 4c. The experimental FT^{-1} spectra present the same features observed in the k^3-weighted $\chi(k)$ spectra (see Figure 4a). In particular, the elongated upward oscillation (6.8 $Å^{-1}$) followed by the splitting of the oscillation with two maxima are clearly visible (7.6 and 8.2 $Å^{1}$), indicating a dependency to the presence, and the type as well as the concentration of earth-alkaline metal ion.

Data fitting was performed in a step-by-step approach using the Liebigite ($Ca_2UO_2(CO_3)_3 \cdot 11H_2O$) [28] crystal model as the starting structure, in which a uranyl tricarbonate species is bound to an unknown number of Ca(II) or Mg(II) ions. Thus, the starting model used during fitting procedure included four shells ($U\text{-}O_{axial}$, $U\text{-}O_{equatorial}$, U-C, $U\text{-}O_{distal}$) for the references sample (UO_2-CO_3) and the Ca/Mg-containing

samples (Ca1, Mg1, Mg2, and Mg3). The fitting approach for the later samples included the subsequent addition of shells (either U-Ca or U-Mg) until the fit quality indicated by the reduced χ^2 and the R-factor did not improve significantly. Furthermore, for the uranyl complexes, the multiple scattering paths arising from the axial and distal oxygen as well as from the carbon show a significant contribution to the fit quality and have to be introduced in the fitting procedure [11, 29] (see Table 1). This model does not sufficiently describe one feature at *ca*. R + ΔR = 3.0 Å, therefore, a further path described by U-C_{distal} was added, which significantly improved the quality of the fit. During fitting procedures, all coordination numbers (CN) were fixed to the values of the Liebigite structure, except for the unknown earth-alkaline metal ions and distal carbon ion.

As observed from the RSF (Figure 4b), the axial and equatorial oxygen atoms are comparable in all samples with distances of 1.80 and 2.45 Å (see Table 2), respectively, indicating a hexagonal bipyramidal coordination, suggesting that the carbon ion lies in the equatorial plane. This is confirmed from the U-C distance of *ca*. 2.90 Å, which is within error comparable in all samples. As further suggested by the RSF, the greatest differences are indicated by the distal shells of the earth alkali and the distal oxygen. The latter shows shorter distances for the Ca-containing sample (Ca1, 4.15 Å) compared to the pure uranyl carbonate (UO_2-CO_3) and the Mg-containing (*ca*. 4.20 Å) samples (Mg1, Mg2, and Mg3). The earth-alkaline metal ions show much shorter distances for the Mg (*ca*. 3.83 Å) compared to the Ca ion (*ca*. 4.15 Å), most probably due to the smaller ionic radius of Mg (0.89 Å) compared to Ca (1.12 Å) [30]. Furthermore, the U-Ca distance calculated in the present work is longer than that in the Liebigite crystal structure (ΔR = 0.1 Å) and very similar to the U-O_{distal} distance. Moreover, Ca indicates large CN (4.5) and high Debye Waller (DW) values (0.012 Å^2), suggesting a larger system disorder. The high system disorder agrees with longer Ca distances than in the Liebigite structure. For the Mg-containing samples, both CN and DW increase with increasing Mg(II) ion concentration, suggesting an increase of disorder, further indicated by the relatively large errors. Overall, the above findings are in good agreement with the Liebigite structure. As stated above, in order to significantly improve the fit quality, a further carbon shell was added to the fit model. This shell shows similar distances (*ca*. 3.48 Å) and CN (*ca*. 3) for all samples, suggesting the presence of a further species comparable to the Rutherfordine (UO_2CO_3) structure although with slightly shorter distance (ΔR = – 0.1 Å) [31]. The DW factor is relatively high, and in some cases had to be fixed, further suggesting a high disorder of this latter species.

Table 1: Description of the paths included in the model and parameters employed in the fitting procedure.

Paths	CN	R (Å)	σ^2 (Å^2)
U-$O_{ax.}$	2	free	free
U-$O_{eq.}$	6	free	free
U-C	3	free	free
U-$C_{dist.}$	free	free	free
U-$O_{ax.1}$-$O_{ax.1}$	2	2 × $O_{ax.}$	4 × $O_{ax.}$
U-$O_{ax.1}$-U-$O_{ax.2}$	2	2 × $O_{ax.}$	2 × $O_{ax.}$
U-$O_{ax.1}$-U-$O_{ax.2}$	2	2 × $O_{ax.}$	2 × $O_{ax.}$
U-Ca	free	free	free
U-Mg	free	free	free
U-$O_{dist.}$	3	free	free
U-C-$O_{dist.}$	6	$O_{dist.}$	$O_{dist.}$
U-C-$O_{dist.}$-C	3	$O_{dist.}$	$O_{dist.}$

CN, coordination number; R, interatomic distance; σ^2, Debye Waller factor; ax., axial; eq., equatorial; dist., distal.

To summarize, the EXAFS data indicate the presence of two species for all samples: a major species with parameters in good agreement with the Liebigite structure and a minor species with a U-C distal shell comparable to the Rutherfordine structure.

3.3 Chemical and thermodynamic models

The slope analysis of the fluorescence intensity against log [Mg(II)] was used to derive the formation constant of ternary Mg-UO_2-CO_3 complexes. Hence, the formation of the first ternary Mg-UO_2-CO_3 species can be described according to the equilibrium reaction and the corresponding equilibrium constant represented in eq. (6) and eq. (7), respectively:

$$x \cdot Mg^{2+} + UO_2(CO_3)_3^{4-} \leftrightarrow Mg_xUO_2(CO_3)_3^{2x-4} \quad (6)$$

$$K_{x13} = \frac{[Mg_xUO_2(CO_3)_3^{2x-4}]}{[Mg^{2+}]^x[UO_2(CO_3)_3^{4-}]} \quad (7)$$

Eq. (7) can be re-arranged to obtain a linear relationship between $\log\frac{[Mg_xUO_2(CO_3)_3^{2x-4}]}{[UO_2(CO_3)_3^{4-}]}$ and log [Mg(II)], where the slope is the stoichiometric number of Mg(II) ions participating in the complexation reaction and the y-intercept is log K_{x13}.

$$x \cdot \log[Mg^{2+}] + \log K_{x13} = \log\frac{[Mg_xUO_2(CO_3)_3^{2x-4}]}{[UO_2(CO_3)_3^{4-}]} \quad (8)$$

Table 2: Structural information obtained from EXAFS U L_{III}-edge data analysis.

Sample	[Me(II)]		Δk (Å^{-1})	ΔR (Å)			U-$O_{ax.}$			U-$O_{eq.}$			U-C				
					CN^x	R (Å)^f	σ^2 (Å^2)^f	CN^x	R (Å)^f	σ^2 (Å^2)^f	CN^x	R (Å)^f	σ^2 (Å^2)^f	CN^x	R (Å)^f	σ^2 (Å^2)^f	
UO_2-CO_3		0 mM	2.75–12.42	1.00–4.35	2.0	1.80(1)	0.002(1)	6.0	2.45(1)	0.007(1)	3.0	2.89(2)	0.006(3)				
Ca1	Ca	6 mM	2.79–12.10	1.00–4.32	2.0	1.80(1)	0.002(1)	6.0	2.45(1)	0.007(1)	3.0	2.90(1)	0.009(1)				
Mg1		10 mM	2.78–12.04	1.00–4.59	2.0	1.80(1)	0.002(1)	6.0	2.46(1)	0.008(1)	3.0	2.89(2)	0.003(2)				
Mg2	Mg	48 mM	2.75–12.04	1.00–4.36	2.0	1.80(1)	0.003(1)	6.0	2.46(1)	0.008(1)	3.0	2.91(2)	0.003(2)				
Mg3		104 mM	2.75–12.48	1.00–4.26	2.0	1.80(1)	0.002(1)	6.0	2.46(1)	0.008(1)	3.0	2.89(2)	0.006(4)				

Sample	U-$C_{dist.}$			U-Ca/Mg			U-$O_{dist.}$			ΔE_0 (eV)^c	N_i	N_v	Reduced χ^2	R-factor
	CN^f	R (Å)^f	σ^2 (Å^2)^f	CN^f	R (Å)^f	σ^2 (Å^2)^f	CN^x	R (Å)^f	σ^2 (Å^2)^f					
UO_2-CO_3	3.4(2.1)	3.46(3)	0.011(12)	–	–	–	3.0	4.21(2)	0.009(2)	6.08(1.08)	20.4	12	321	0.018
Ca1	2.3(1.0)	3.49(2)	0.001(4)	4.5(2.2)	4.15(3)	0.012(1)	3.0	4.15(2)	0.003(3)	6.72(0.9)	19.3	15	239	0.011
Mg1	2.7(9)	3.48(3)	0.005^x	0.8(1.6)	3.82(7)	0.002(17)	3.0	4.21(2)	0.011(3)	7.58(1.06)	20.8	11	613	0.034
Mg2	2.9(9)	3.48(3)	0.005^x	0.7(1.0)	3.82(11)	0.003(28)	3.0	4.20(2)	0.009(2)	7.22(1.07)	19.6	11	829	0.028
Mg3	2.8(9)	3.50(4)	0.006(10)	1.4(1.1)	3.84(6)	0.010(10)	3.0	4.20(2)	0.006(2)	7.27(1.16)	21.7	13	519	0.023

x, Fixed parameters; f, free parameters; c, correlated parameters; Δk and ΔR, intervals of the filtering windows used for the forward and back-fourier transformations; CN, coordination number; R, interatomic distance; σ^2, Debye Waller factor; ΔE_0, shift of threshold energy; N_i, number of independent points; N_v, number of variables; $S_0^2 = 1$, errors are shown in brackets and indicate the variations of the last numbers.

Since both U(VI) species with and without complexed Mg(II) ions emit considerable fluorescence signals, the relative concentration ratio of both fluorescent $UO_2(CO_3)_3^{4-}$ and $Mg_xUO_2(CO_3)_3^{2x-4}$ species was estimated based on fluorescence intensity coupled with fluorescence intensity factor. The fluorescence intensities at gate delay time $\Delta t_d = 0$ and at gate width $\Delta t_w = 50$ ns as a function of Mg(II) ion concentration were utilized for further analysis.

As described in eq. (9), the relationship between fluorescence intensity and concentration of fluorescent chemical species is defined in terms of the fluorescence intensity factor: [32]

$$FI_x = (k \cdot I_0 \cdot l)(\eta_x \cdot \varepsilon_x) \cdot C_x = \nu_x \cdot C_x \tag{9}$$

where the first term represents the experimental set-up regarding the proportionality factor k, the intensity of laser I_0, and the optical pathlength l. The second term indicates the fluorescence efficiency of fluorescent species in terms of the molar absorption coefficient ε_x and the fluorescence quantum yield η_x. The fluorescence intensity factor ν_x can be determined from the ratio between the fluorescence intensity FI_x and the concentration of fluorescent species C_x.

Under the justified assumption that the fluorescence intensity factor remains constant, the concentration ratio of $UO_2(CO_3)_3^{4-}$ and $Mg_xUO_2(CO_3)_3^{2x-4}$ species can be described with FI_x and ν_x, as expressed in eqs. (10), (11) and (12):

$$x \cdot \log[Mg^{2+}] + \log K_{x13} = \log \frac{\nu_{UO_2(CO_3)_3^{4-}} \cdot FI_{Mg_xUO_2(CO_3)_3^{2x-4}}}{\nu_{Mg_xUO_2(CO_3)_3^{2x-4}} \cdot FI_{UO_2(CO_3)_3^{4-}}} \tag{10}$$

$$= \log \frac{FI_{Mg_xUO_2(CO_3)_3^{2x-4}}}{FI_{UO_2(CO_3)_3^{4-}}} - \log \frac{\nu_{Mg_xUO_2(CO_3)_3^{2x-4}}}{\nu_{UO_2(CO_3)_3^{4-}}} \tag{11}$$

$$= \log R \tag{12}$$

At the same time, the formation of the second Mg-UO_2-CO_3 species can be described according to the relevant equilibrium reaction and the stepwise formation constant, as expressed below:

$$y \cdot Mg^{2+} + Mg_xUO_2(CO_3)_3^{2x-4} \leftrightarrow Mg_zUO_2(CO_3)_3^{2z-4} \tag{13}$$

$$K_{z13} = \frac{[Mg_zUO_2(CO_3)_3^{2z-4}]}{[Mg^{2+}]^y [Mg_xUO_2(CO_3)_3^{2x-4}]} \tag{14}$$

$$= \frac{[Mg_zUO_2(CO_3)_3^{2z-4}]}{K_{x13}[Mg^{2+}]^z [UO_2(CO_3)_3^{4-}]} \tag{15}$$

where y indicates the number of Mg(II) ions participating in the complexation reaction between Mg(II) ions

and $Mg_xUO_2(CO_3)_3^{2x-4}$ and z represents the stoichiometric number of total Mg(II) ions bound to the second Mg-UO_2-CO_3 species, which is equal to x + y. For the first Mg-UO_2-CO_3 species, a linear relationship between the concentration ratio of U(VI) carbonate complexes and log [Mg(II)] can be achieved by taking logarithms of both sides of eqs. (14) and (15) and relevant fluorescence intensity factors:

$$y \cdot \log[Mg^{2+}] + \log K_{z13} = \log \frac{[Mg_zUO_2(CO_3)_3^{2z-4}]}{[Mg_xUO_2(CO_3)_3^{2x-4}]} \quad (16)$$

$$= \log \frac{\nu_{Mg_xUO_2(CO_3)_3^{2x-4}} \cdot FI_{Mg_zUO_2(CO_3)_3^{2z-4}}}{\nu_{Mg_zUO_2(CO_3)_3^{2z-4}} \cdot FI_{Mg_xUO_2(CO_3)_3^{2x-4}}} \quad (17)$$

$$= \log \frac{FI_{Mg_zUO_2(CO_3)_3^{2z-4}}}{FI_{Mg_xUO_2(CO_3)_3^{2x-4}}} - \log \frac{\nu_{Mg_zUO_2(CO_3)_3^{2z-4}}}{\nu_{Mg_xUO_2(CO_3)_3^{2x-4}}} \quad (18)$$

$$= \log Q \quad (19)$$

$$z \cdot \log[Mg^{2+}] + \log K_{z13} + \log K_{x13} = \log \frac{[Mg_zUO_2(CO_3)_3^{2z-4}]}{[UO_2(CO_3)_3^{4-}]} \quad (20)$$

$$= \log \frac{\nu_{UO_2(CO_3)_3^{4-}} \cdot FI_{Mg_zUO_2(CO_3)_3^{2z-4}}}{\nu_{Mg_zUO_2(CO_3)_3^{2z-4}} \cdot FI_{UO_2(CO_3)_3^{4-}}} \quad (21)$$

$$= \log \frac{FI_{Mg_zUO_2(CO_3)_3^{2z-4}}}{FI_{UO_2(CO_3)_3^{4-}}} - \log \frac{\nu_{Mg_zUO_2(CO_3)_3^{2z-4}}}{\nu_{UO_2(CO_3)_3^{4-}}} \quad (22)$$

$$= \log P \quad (23)$$

By fitting the fluorescence decay curves, the FI_0 values (see eq. (4)) for the three different uranium species are obtained which can be transferred to relative fluorescence intensity values presented in Table 3. Sequentially, the least square method [33] was utilized to calculate fluorescence intensity factors of each uranium complex considering the total uranium concentration in all uranium sample sets. Table 3 shows the fluorescence intensity ratios and fluorescence intensity factors of each uranium species obtained at various Mg(II) ion concentrations.

For determining the stoichiometric number of Mg(II) ion bound to the Mg-UO_2-CO_3 species, log R, log Q, and log P values obtained at different ionic strengths were corrected to infinitely diluted solution (I = 0 M) according to the SIT, [22, 23] as described in the experimental section. Figure 5a presents log R values determined based on the

Table 3: Fluorescence intensity ratios and fluorescence intensity factors of uranium carbonate complexes.

[Mg(II)] (mmol/L)	Fluorescence intensity ratio		
	$UO_2(CO_3)_3^{4-}$	First U(VI) species	Second U(VI) species
1.7	83%	16%	< 1%
4.2	67%	32%	1%
8.7	53%	44%	3%
17.0	34%	61%	5%
39.2	11%	80%	9%
FL lifetime (ns)	9 ± 1	17 ± 2	51 ± 2
FI factor (count/(mol/L))	3.78×10^{11}	6.58×10^{11}	1.68×10^{12}

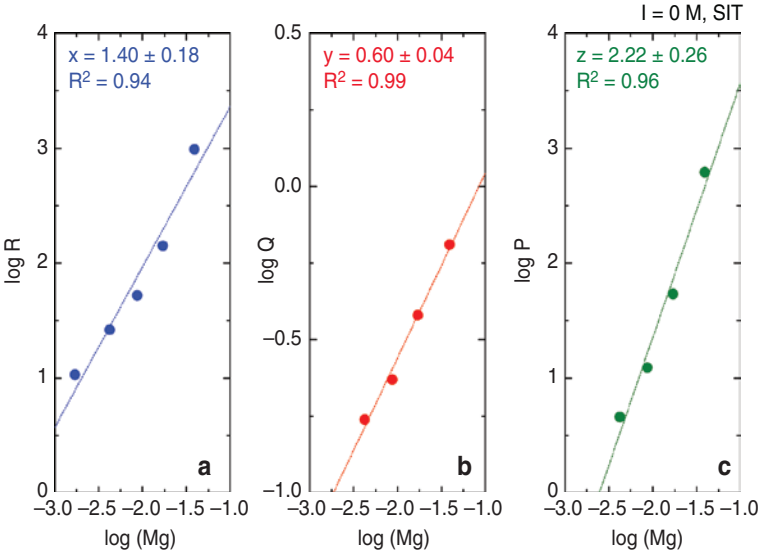

Figure 5: (a) log R, (b) log Q, and (c) log P values evaluated with fluorescence intensity ratios and fluorescence intensity factors of each uranium carbonate species as a function of log [Mg(II)] at pH = 8.2.

fluorescence intensity ratios and fluorescence intensity factors of each uranium carbonate complex at various Mg(II) ion concentrations (Table 3), indicating the relative concentration ratio between uncomplexed uranium carbonate species and the first Mg-UO_2-CO_3 species. The slope of the linear fit was evaluated to be 1.40 ± 0.18, representing the formation of $MgUO_2(CO_3)_3^{2-}$ species in the given Mg(II) ion concentration range. Note that this approach uses $[Mg^{2+}]_{free} = [Mg^{2+}]_{tot}$.

The log Q values as a function of log [Mg(II)] are illustrated in Figure 5b. The fluorescence intensity ratio is not considered for the sample with the lowest Mg(II) ion concentration showing a low fluorescence yield (<1%) of the second Mg-UO_2-CO_3 species. The linear fit of log Q provides one single linear slope of 0.60 ± 0.04, indicating that approximately one Mg(II) ion is additionally bound to the $MgUO_2(CO_3)_3^{2-}$ species to form the $Mg_2UO_2(CO_3)_3(aq)$ species. At the same time, the log P values were complementarily calculated from the logarithms of the relative concentration ratios between the secondly formed Mg-UO_2-CO_3 species and uncomplexed uranium carbonate species, as shown in Figure 5c. Based on the eq. (23), a linear fit of log P against log [Mg(II)] reveals the z value, which represents the stoichiometric number of total Mg(II) ions in the second Mg-UO_2-CO_3 complex. The z value is evaluated to be 2.22 ± 0.26, based on the slope of the linear fit, indicating the formation of the $Mg_2UO_2(CO_3)_3(aq)$ species. According to the result, both log Q and log P values are evidently indicating the presence of the $Mg_2UO_2(CO_3)_3(aq)$ species.

Since the slopes of the linear fits are not whole numbers, the intercepts of the linear fits of eqs. (12), (19), and (23) deviate from the formation constants of the ternary Mg-UO_2-CO_3 complexes. Thus, the value of x, y, and z rounded off to the nearest integer ($x = 1$, $y = 1$, and $z = 2$) are assumed for the calculation of the stepwise formation constants in the present work. As shown in Table 4, the stepwise formation constants of $MgUO_2(CO_3)_3^{2-}$ and $Mg_2UO_2(CO_3)_3(aq)$ at $I = 0$ M are determined to be $\log K^0_{113} = 3.9 \pm 0.3$ and $\log K^0_{213} = 1.4 \pm 0.2$ at $pH = 8.2$. However, due to the relatively small fractions of $Mg_2UO_2(CO_3)_3(aq)$ species (<10%) in the conditions of the present study, the uncertainty associated to $\log K^0_{213}$ was increased to ± 0.3. Accordingly, the formation constants of those species are calculated as $\log \beta^0_{113} = 25.8 \pm 0.3$ and $\log \beta^0_{213} = 27.1 \pm 0.6$ by considering uncertainty propagation.

The spectroscopic properties and chemical thermodynamic data of Mg-UO_2-CO_3 complexes obtained are in good accordance with other literature data [2, 9, 10]. The data of the $Mg_2UO_2(CO_3)_3(aq)$ species is reported for the first time to our knowledge (see Table 5).

3.4 Aqueous speciation of U(VI) in seawater

The distribution of U(VI) species was calculated under carbonate-saturated condition at $I = 0.5$ M (equilibrated with atmospheric $CO_2(g)$) according to the formation constants of Mg-UO_2-CO_3 species obtained in the present work and other uranium species reported in Table A1. The formation of both Ca-UO_2-CO_3 and Mg-UO_2-CO_3 complexes was considered for the chemical speciation calculations because of significant concentrations of Ca(II) and Mg(II) ions in seawater condition. The concentrations of earth-alkaline metal ions were initially set to be $[Ca(II)] = 0.011$ M and $[Mg(II)] = 0.055$ M according to the standard seawater composition [3] reported by Millero et al. Carbonate concentration in the calculations was set to $pCO_2 = 10^{-3.5}$ atm. As illustrated in Figure 6, the calculation shows noticeable formation of $MgUO_2(CO_3)_3^{2-}$ species particularly at neutral pH even with relatively low formation constant of $MgUO_2(CO_3)_3^{2-}$ species ($\log \beta^0 = 25.8 \pm 0.3$) compared to $CaUO_2(CO_3)_3^{2-}$ species ($\log \beta^0 = 27.27 \pm 0.14$) [8]. Thus, considerable presence of $MgUO_2(CO_3)_3^{2-}$ species was observed, which is also suggested by the higher

Table 4: Conditional stepwise formation constants of $Mg_xUO_2(CO_3)_3^{2x-4}$ complexes determined in this work at various Mg(II) ion concentrations and ionic strengths, and corresponding extrapolation to $I = 0$ M using the extended SIT approach described in the experimental section.

Species			$MgUO_2(CO_3)_3^{2-}$		$Mg_2UO_2(CO_3)_3(aq)$			
[Mg(II)] (mmol/L)	[Na] (mol/L)	I (M)	$\log K'_{113}$	$\log K^0_{113}$	$\log K'_{213}$		$\log K^0_{213}$	
1.7	0.11	0.15	1.8	3.8	–	–	–	–
4.2	0.11	0.15	1.8	3.8	0.6[a]	0.5[b]	1.6[a]	1.5[b]
8.7	0.10	0.17	1.7	3.8	0.5[a]	0.3[b]	1.4[a]	1.3[b]
17.0	0.10	0.20	1.8	3.9	0.3[a]	0.3[b]	1.3[a]	1.4[b]
39.2	0.10	0.29	2.0	4.4	0.2[a]	0.6[b]	1.2[a]	1.7[b]
Average			–	3.9 ± 0.3		–		1.4 ± 0.3[c]

[a]Derived from log Q values; [b]derived from log P values; [c]the uncertainty was re-assessed by the authors.

Table 5: Spectroscopic properties and chemical thermodynamic data of Mg-UO_2-CO_3 complexes.

Species	FL wavelength (nm)	FL lifetime (ns)	log β^0
$UO_2(CO_3)_3^{4-}$	467-485-506-528-551[a]	9 ± 1[a]	n.d.
	466-485-505-526-549 [8]	11.6 ± 0.1 [8]	n.d.
	468-487-507-529-551 [27]	6–12 [27]	n.d.
	468-485-506-527-551 [34]	8.9 ± 0.8 [34]	n.d.
$MgUO_2(CO_3)_3^{2-}$	467-485-506-528-551[a]	17 ± 2[a]	25.8 ± 0.3[a]
	466-485-505-527-551 [2]	18.2 ± 2.7 [2]	26.24 ± 0.13 [2]
	n.d.	n.d.	26.11 ± 0.04 [9]
	n.d.	n.d.	26.25 ± 0.04 [10]
$Mg_2UO_2(CO_3)_3(aq)$	467-485-506-528-551[a]	51 ± 2[a]	27.1 ± 0.6[a]

[a]Present work; n.d., not determined.

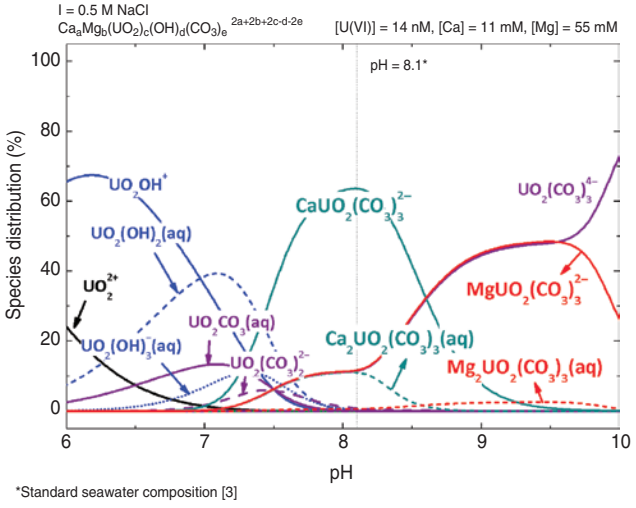

Figure 6: The species distribution of aqueous U(VI) complexes at $[U(VI)] = 10^{-4}$ M, $[Ca(II)] = 1.1 \times 10^{-2}$ M, $[Mg(II)] = 5.5 \times 10^{-2}$ M, $[U(VI)] = 1.4 \times 10^{-8}$ M, I = 0.5 M NaCl, and $pCO_2 = 10^{-3.5}$ atm based on the formation constants of Mg-UO_2-CO_3 species obtained in the present work and the formation constants of other U(VI) species reported in literatures. Minor U(VI) species are not shown.

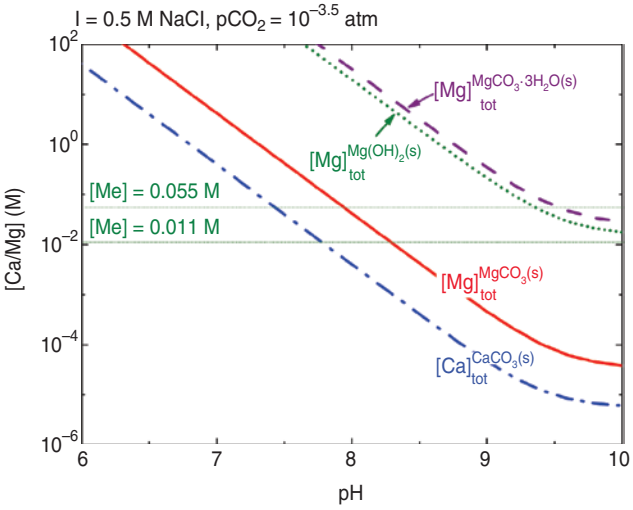

Figure 7: The solubility of earth-alkaline metal ions at I = 0.5 M NaCl and $pCO_2 = 10^{-3.5}$ atm calculated based on the formation constants of chemical species obtained from the literature [21].

solubility product of $MgCO_3 \cdot 3H_2O$(s) compared to $CaCO_3$(s) providing more Mg(II) free ion (see Figure 7) in order to form the Mg-UO_2-CO_3 species. In addition, especially at low ionic strength conditions (I < 0.01 M), considerable formation of $Ca_2UO_2(CO_3)_3$(aq) species is expected in the presence of millimolar concentrations of Ca at neutral to weakly alkaline conditions. Under analogous conditions, a minor contribution of the $Mg_2UO_2(CO_3)_3$(aq) species is expected due to the low stability constant of the second Mg-UO_2-CO_3 species (log $\beta^0 = 27.1 \pm 0.6$) compared to the analog $Ca_2UO_2(CO_3)_3$(aq) species (log $\beta^0 = 29.81 \pm 0.19$) [8]. According to the chemical thermodynamic data, sub-molar concentrations of Mg(II) ion are required to form $Mg_2UO_2(CO_3)_3$(aq) species in aqueous solution.

However, as represented in Figure 7, under strongly alkaline pH conditions where the concentration of both Mg(II) and Ca(II) decreases due to the precipitation of $MgCO_3 \cdot 3H_2O$(s) (and/or $Mg(OH)_2$(s)) and $CaCO_3$(s), respectively, the predominance of $UO_2(CO_3)_3^{4-}$ was predicted.

4 Conclusions

The spectroscopic properties and chemical behavior of Mg-UO_2-CO_3 species were investigated by TRLFS and EXAFS. The formation of ternary Mg-UO_2-CO_3 species was identified in terms of fluorescence intensity with increasing Mg(II) ion concentrations at weakly alkaline conditions. The laser spectroscopic characteristics of both $MgUO_2(CO_3)_3^{2-}$ and $Mg_2UO_2(CO_3)_3$(aq) species are almost identical with each other, except for the fluorescence lifetimes of 17 ± 2 ns and 51 ± 2 ns for $MgUO_2(CO_3)_3^{2-}$ and $Mg_2UO_2(CO_3)_3$(aq), respectively. The remarkable difference in fluorescence lifetimes results in a multi-exponential

fluorescence decay function, which allows the unequivocal identification and quantification of the two Mg-UO_2-CO_3 species.

The slope analysis in terms of fluorescence intensity coupled with the fluorescence intensity factor was used to characterize the exact chemical behavior of Mg(II)-bound U(VI) carbonate species. The conditional formation constants for both $MgUO_2(CO_3)_3^{2-}$ and $Mg_2UO_2(CO_3)_3(aq)$ species were extrapolated to I = 0 M using the SIT approach ($\log \beta^0_{113} = 25.8 \pm 0.3$ and $\log \beta^0_{213} = 27.1 \pm 0.6$) and considering $\varepsilon(MgUO_2(CO_3)_3^{2-}, Na^+) = -0.02 \pm 0.09$ kg·mol^{-1} and $\varepsilon(Mg_2UO_2(CO_3)_3(aq), Na^+) = 0$ kg·mol^{-1}, respectively.

The spectroscopic properties and chemical thermodynamic characteristics of the $MgUO_2(CO_3)_3^{2-}$ species match well with reported literature [2, 9, 10]. To the best of our knowledge, this is the first study reporting the formation of the higher $Mg_2UO_2(CO_3)_3(aq)$ species, which has a significantly lower stability than the corresponding Ca-counterpart.

Results from the X-ray absorption spectroscopic analysis indicate the formation of Mg-UO_2-CO_3 species similar to the Liebigite structure. The shorter U-Mg distance compared to the U-Ca distance can be associated with different ionic radii. Furthermore, a minor uranyl species could be identified, as indicated by the carbon ion at longer distance (3.48 Å). The presence of this latter species is independent of the earth-alkaline metal ion and their concentrations.

In seawater media, the formation of Mg-UO_2-CO_3 species considerably influences the aqueous U(VI) species distribution especially at neutral pH even in the presence of Ca(II) ion. In seawaters with relatively low free Ca(II) ions compared with the concentration of free Mg(II) ions at neutral to weakly alkaline pH condition, a noticeable formation of $MgUO_2(CO_3)_3^{2-}$ species is expected.

Acknowledgement: This work was supported by the Nuclear Safety Research Program (1305032-0315-CG100) through the Korea Foundation of Nuclear Safety (KOFONS), granted financial resource from the Nuclear Safety and Security Commission (NSSC), Republic of Korea. Petra Panak, Andrej Skerencak-Frech, and Daniel Fröhlich (University of Heidelberg) are kindly acknowledged for the technical support with the TRLFS measurements. The help of Melanie Böttle and Cornelia Walschburger (KIT-INE) with ICP-OES and ICP-MS measurements is highly appreciated. Finally, the authors are indebted to Seonggyu Choi (KAIST) for the MATLAB code calculation.

Appendix

Table A1: Formation constants of U(VI) species at 25°C and I = 0 M obtained from the OECD-NEA thermodynamic database [20] and other literatures [8, 21].

Reaction	$\log \beta^0$
$UO_2^{2+} + H_2O(l) \leftrightarrow UO_2OH^+ + H^+$	-5.25 ± 0.24 [20]
$UO_2^{2+} + 2H_2O(l) \leftrightarrow UO_2(OH)_2(aq) + 2H^+$	-12.15 ± 0.07 [20]
$UO_2^{2+} + 3H_2O(l) \leftrightarrow UO_2(OH)_3^- + 3H^+$	-20.25 ± 0.42 [20]
$UO_2^{2+} + 4H_2O(l) \leftrightarrow UO_2(OH)_4^{2-} + 4H^+$	-32.40 ± 0.68 [20]
$2UO_2^{2+} + H_2O(l) \leftrightarrow (UO_2)_2OH^{3+} + H^+$	-2.70 ± 1.00 [20]
$2UO_2^{2+} + 2H_2O(l) \leftrightarrow (UO_2)_2(OH)_2^{2+} + 2H^+$	-5.62 ± 0.04 [20]
$3UO_2^{2+} + 4H_2O(l) \leftrightarrow (UO_2)_3(OH)_4^{2+} + 4H^+$	-11.90 ± 0.30 [20]
$3UO_2^{2+} + 5H_2O(l) \leftrightarrow (UO_2)_3(OH)_5^+ + 5H^+$	-15.55 ± 0.12 [20]
$3UO_2^{2+} + 7H_2O(l) \leftrightarrow (UO_2)_3(OH)_7^- + 7H^+$	-32.20 ± 0.80 [20]
$4UO_2^{2+} + 7H_2O(l) \leftrightarrow (UO_2)_4(OH)_7^+ + 7H^+$	-21.90 ± 1.00 [20]
$UO_2^{2+} + CO_3^{2-} \leftrightarrow UO_2CO_3(aq)$	9.94 ± 0.03 [20]
$UO_2^{2+} + 2CO_3^{2-} \leftrightarrow UO_2(CO_3)_2^{2-}$	16.61 ± 0.09 [20]
$UO_2^{2+} + 3CO_3^{2-} \leftrightarrow UO_2(CO_3)_3^{4-}$	21.84 ± 0.04 [20]
$3UO_2^{2+} + 6CO_3^{2-} \leftrightarrow (UO_2)_3(CO_3)_6^{6-}$	54.00 ± 1.00 [20]
$Ca^{2+} + UO_2^{2+} + 3CO_3^{2-} \leftrightarrow CaUO_2(CO_3)_3^{2-}$	27.27 ± 0.14 [8]
$2Ca^{2+} + UO_2^{2+} + 3CO_3^{2-} \leftrightarrow Ca_2UO_2(CO_3)_3(aq)$	29.81 ± 0.19 [8]
$Mg^{2+} + H_2O(l) \leftrightarrow MgOH^+ + H^+$	-11.44 [21]
$Mg^{2+} + HCO_3^- \leftrightarrow MgHCO_3^+$	1.07 [21]
$Mg^{2+} + CO_3^{2-} \leftrightarrow MgCO_3(aq)$	2.98 [21]
$Ca^{2+} + H_2O(l) \leftrightarrow CaOH^+ + H^+$	-12.78 [21]

Table A1 (continued)

Reaction	log β^0
$Ca^{2+} + HCO_3^- \leftrightarrow CaHCO_3^+$	1.106 [21]
$Ca^{2+} + CO_3^{2-} \leftrightarrow CaCO_3$(aq)	3.224 [21]
$UO_3 \cdot 2H_2O$(cr) $\leftrightarrow UO_2^{2+} + 2OH^- + H_2O$(l)	− 23.19 ± 0.43 [20]
$0.5Na_2U_2O_7$(cr) + $1.5H_2O$(l) $\leftrightarrow UO_2^{2+} + 3OH^- + Na^+$	− 30.7 ± 0.5 [20]
UO_2CO_3(cr) $\leftrightarrow UO_2^{2+} + CO_3^{2-}$	− 14.76 ± 0.02 [20]
$CaU_6O_{19} \cdot 11H_2O$(cr) + $14H^+ \leftrightarrow 6UO_2^{2+} + Ca^{2+} + 18H_2O$(l)	40.5 ± 1.6 [20]
$MgCO_3$(s) $\leftrightarrow Mg^{2+} + CO_3^{2-}$	− 7.46 [21]
$MgCO_3 \cdot 3H_2O$(s) $\leftrightarrow Mg^{2+} + CO_3^{2-} + 3H_2O$(l)	− 4.67 [21]
$Mg(OH)_2$(brucite) + $2H^+ \leftrightarrow Mg^{2+} + 2H_2O$(l)	16.84 [21]
$CaCO_3$(s) $\leftrightarrow Ca^{2+} + CO_3^{2-}$	− 8.48 [21]
$Ca(OH)_2$(portlandite) + $2H^+ \leftrightarrow Ca^{2+} + 2H_2O$(l)	22.8 [21]

Table A2: Specific ion interaction coefficients (ε) of major chemical species at 25°C obtained from the OECD-NEA thermodynamic database [20].

Species	ε (kg·mol^{-1}, Na^+)	ε (kg·mol^{-1}, Cl^-)
H^+	–	0.12 ± 0.01
UO_2^{2+}	–	0.21 ± 0.02
Ca^{2+}	–	0.14 ± 0.01
Mg^{2+}	–	0.19 ± 0.02
OH^-	0.04 ± 0.01	–
HCO_3^-	0.00 ± 0.02	–
CO_3^{2-}	− 0.08 ± 0.03	–
UO_2OH^+	–	0.04 ± 0.07[a]
$UO_2(OH)_2$(aq)	0[b]	0[a]
$UO_2(OH)_3^-$	− 0.09 ± 0.05	–
$UO_2(OH)_4^{2-}$	− 0.02 ± 0.09[a]	–
$(UO_2)_2OH^{3+}$	–	0.50 ± 0.05[a]
$(UO_2)_2(OH)_2^{2+}$	–	0.69 ± 0.07
$(UO_2)_3(OH)_4^{2+}$	–	0.50 ± 0.18
$(UO_2)_3(OH)_5^+$	–	0.81 ± 0.17
$(UO_2)_3(OH)_7^-$	− 0.09 ± 0.05[a]	–
$(UO_2)_4(OH)_7^+$	–	0.81 ± 0.17[a]
UO_2CO_3(aq)	0[b]	0[b]
$UO_2(CO_3)_2^{2-}$	− 0.02 ± 0.09	–
$UO_2(CO_3)_3^{4-}$	− 0.01 ± 0.11	–
$(UO_2)_3(CO_3)_6^{6-}$	0.37 ± 0.11	–
$CaUO_2(CO_3)_3^{2-}$	− 0.02 ± 0.09[c]	–
$Ca_2UO_2(CO_3)_3$(aq)	0[a]	0[a]
$MgUO_2(CO_3)_3^{2-}$	− 0.02 ± 0.09[c,d]	–
$Mg_2UO_2(CO_3)_3$(aq)	0[a]	0[a]

a, Estimated by charge analogy; b, by definition set to zero in SIT; c, in analogy with ε($UO_2(CO_3)_2^{2-}$, Na^+) selected in the NEA-TDB; d, ε($MgUO_2(CO_3)_3^{2-}$, Mg^{2+}) = 0.0 ± 0.2 kg·mol^{-1}, estimated in this work (see text).

References

1. Kim, J. I., Grambow, B.: Geochemical assessment of actinide isolation in a german salt repository environment. Eng. Geol. **52**, 221 (1999).
2. Geipel, G., Amayri, S., Bernhard, G.: Mixed complexes of alkaline earth uranyl carbonates: a laser-induced time-resolved fluorescence spectroscopic study. Spectrochim. Acta Part A **71**, 53 (2008).
3. Millero, F. J., Feistel, R., Wright, D. G., McDougall, T. J.: The composition of standard seawater and the definition of the reference-composition salinity scale. Deep Sea Res. Part I **55**, 50 (2008).
4. Choi, B.-Y., Kim, G.-Y., Koh, Y.-K., Shin, S.-H., Yoo, S.-W., Kim, D.-H.: Geochemical characteristics of a LILW repository I. Groundwater. J. Korean Radioact. Waste Soc. **6**, 297 (2008).
5. Bernhard, G., Geipel, G., Brendler, V., Nitsche, H.: Speciation of uranium in seepage waters of a mine tailing pile studied by time-resolved laser-induced fluorescence spectroscopy (TRLFS). Radiochim. Acta **74**, 87 (1996).
6. Kalmykov, S. N., Choppin, G. R.: Mixed $Ca^{2+}/UO_2^{2+}/CO_3^{2-}$ complex formation at different ionic strengths. Radiochim. Acta **88**, 603 (2000).
7. Bernhard, G., Geipel, G., Reich, T., Brendler, V., Amayri, S., Nitsche, H.: Uranyl(VI) carbonate complex formation: validation of the $Ca_2UO_2(CO_3)_3$(aq.) species. Radiochim. Acta **89**, 511 (2001).
8. Lee, J.-Y., Yun, J.-I.: Formation of ternary $CaUO_2(CO_3)_3^{2-}$ and $Ca_2UO_2(CO_3)_3$(aq) complexes under neutral to weakly alkaline conditions. Dalton Trans. **42**, 9862 (2013).
9. Dong, W., Brooks, S. C.: Determination of the formation constants of ternary complexes of uranyl and carbonate with alkaline earth metals (Mg^{2+}, Ca^{2+}, Sr^{2+}, and Ba^{2+}) using anion exchange method. Environ. Sci. Technol. **40**, 4689 (2006).
10. Endrizzi, F., Rao, L.: Chemical speciation of uranium(VI) in marine environments: complexation of calcium and magnesium ions with $[(UO_2)(CO_3)_3]^{(4-)}$ and the effect on the extraction of uranium from seawater. Chem. Eur. J. **20**, 14499 (2014).
11. Kelly, S. D., Kemner, K. M., Brooks, S. C., Fredrickson, J. K., Carroll, S. L., Kennedy, D. W., Zachara, J. M., Plymale, A. E., Fendorf, S.: Ca-UO_2-CO_3 complexation – implications for bioremediation of U(VI). Phys. Scr. **T115**, 915 (2005).
12. Tamada, M., Seko, N., Kasai, N., Shimizu, T.: Cost estimation of uranium recovery from seawater with system of braid type adsorbent. Transactions At. Energy Soc. Jpn. **5**, 358 (2006).
13. Kerisit, S., Liu, C.: Molecular simulation of the diffusion of uranyl carbonate species in aqueous solution. Geochim. Cosmochim. Acta **74**, 4937 (2010).

14. Hänchen, M., Prigiobbe, V., Baciocchi, R., Mazzotti, M.: Precipitation in the Mg-carbonate system – effects of temperature and CO_2 pressure. Chem. Eng. Sci. **63**, 1012 (2008).
15. Brendebach, B., Dardenne, K., Denecke, M. A., Rothe, J., Vitova, T.: New developments at the INE-beamline for actinide research at ANKA. Nucl. Instrum. Methods Phys. Res. Sect. A **582**, 80 (2007).
16. Newville, M.: IFFEFFIT: Interactive XAFS analysis and FEFF fitting. J. Synchrotron Radiat. **8**, 322 (2001).
17. Ravel, B., Newville, M.: ATHENA and ARTEMIS: data analysis for X-ray absorption spectroscopy using IFEFFIT. J. Synchrotron Radiat. **12**, 537 (2005).
18. Ankundinov, A. L., Bouldin, C. E., Rehr, J. J., Sims, J., Hung, H.: Parallel calculation of electron multiple scattering using lanczos algorithms. Phys. Rev. B Condens. Matter Mater. Phys. **65**, 104107 (2002).
19. Kelly, S. D., Kemner, K. M., Brooks, S. C.: X-ray absorption spectroscopy identifies calcium-uranyl-carbonate complexes at environmental concentrations. Geochim. Cosmochim. Acta **71**, 821 (2007).
20. Guillaumont, R., Fanghänel, T., Neck, V., Fuger, J., Palmer, D. A., Grenthe, I. and Rand, M. H.: Update on the Chemical Thermodynamics of Uranium, Neptunium, Plutonium, Americium and Technetium. Elsevier, OECD-NEA, Amsterdam (2003).
21. Stumm, W., Morgan, J. J.: Aquatic Chemistry, 3rd ed., John Wiley & Sons, New York (1996).
22. Ciavatta, L.: The specific interaction theory in evaluating ionic equilibria. Ann. Chim. (Rome, Italy) **70**, 551 (1980).
23. Grenthe, I., Wanner, H. and Östhols, E.: Guidelines for the Extrapolation to Zero Ionic Strength. OECD-NEA, Paris (2000).
24. Altmaier, M., Neck, V., Fanghänel, T.: Solubility of Zr(IV), Th(IV) and Pu(IV) hydrous oxides in $CaCl_2$ solutions and the formation of ternary Ca-M(IV)-OH complexes. Radiochim. Acta **96**, 541 (2008).
25. Moulin, C., Laszak, I., Moulin, V., Tondre, C.: Time-resolved laser-induced fluorescence as a unique tool for low-level uranium speciation. Appl. Spectrosc. **52**, 528 (1998).
26. Demtröder, W.: Laser Spectroscopy, 2nd ed., Springer, New York (1998).
27. Götz, C., Geipel, G., Bernhard, G.: The Influence of the temperature on the carbonate complexation of uranium(VI): a spectroscopic study. J. Radioanal. Nucl. Chem. **287**, 961 (2011).
28. Mereiter, K.: The crystal structure of Liebigite, $Ca_2UO_2(CO_3)_3{\sim}11H_2O$. Mineral. Petrol. **30**, 277 (1982).
29. Hudson, E. A., Allen, P. G., Terminello, L. J.: Polarized X-ray-absorption spectroscopy of the uranyl ion: comparison of experiment and theory. Phys. Rev. B Condens. Matter **54**, 156 (1996).
30. Shannon, R. D.: Revised effective ionic radii and systematic studies of interatomic distances in halides and chalocogenides. Acta Crystall. A **32**, 751 (1976).
31. Finch, R. J., Cooper, M. A., Hawthorne, F. C., Ewing, R. C.: Refinement of the crystal structure of Rutherfordine. Can. Mineral. **37**, 929 (1999).
32. Eliet, V., Bidoglio, G., Omenetto, N., Parma, L., Grenthe, I.: Characterisation of hydroxide complexes of uranium(VI) by time-resolved fluorescence spectroscopy. J. Chem. Soc. Faraday Trans. **91**, 2275 (1995).
33. Anton, H. and Busby, R. C.: Contemporary Linear Algebra. Wiley, New York (2003).
34. Jung, E. C., Cho, H.-R., Baik, M. H., Kim, H., Cha, W.: Time-resolved laser fluorescence spectroscopy of $UO_2(CO_3)_3^{4-}$ Dalton Trans. **44**, 18831 (2015).